Article

# Confined Water Dynamics in the Scaffolds of Polylactic Acid

Mariana Ishikawa, Roger Borges, André Mourão, Letície Mendonça Ferreira, Anderson O. Lobo, and Herculano Martinho*

Read Online

ACCESS | Metrics & More | Article Recommendations

**ABSTRACT:** Resorbable polylactic acid (PLA) ultrathin fibers have been applied as scaffolds for tissue engineering applications due to their micro- and nanoporous structure that favor cell adhesion, besides inducing cell proliferation and upregulating gene expression related to tissue regeneration. Incorporation of multiwalled carbon nanotubes into PLA fibers has been reported to increase the mechanical properties of the scaffold, making them even more suitable for tissue engineering applications. Ideally, scaffolds should be degraded simultaneously with tissue growth. Hydration and swelling are factors related to scaffold degradation. Hydration would negatively impact the mechanical properties since PLA shows hydrolytic degradation. Water absorption critically affects the catalysis and allowance of the hydrolysis reactions. Moreover, either mass transport and chemical reactions are influenced by confined water, which is an unexplored subject for PLA micro- and nanoporous fibers. Here, we probe and investigate confined water onto highly porous PLA microfibers containing few amounts of incorporated carbon nanotubes by Fourier transform infrared (FTIR) spectroscopy. A hydrostatic pressure was applied to the fibers to enhance the intermolecular interactions between water molecules and C=O groups from polyester bonds, which were evaluated over the wavenumber between 1600 and 2000 cm$^{-1}$. The analysis of temperature dependence of FTIR spectra indicated the presence of confined water which is characterized by a non-Arrhenius to Arrhenius crossover at $T_0 = 190$ K for 1716 and 1817 cm$^{-1}$ carbonyl bands of PLA. These bands are sensitive to a hydrogen bond network of confined water. The relevance of our finding relies on the challenge detecting confined water in hydrophobic cavities as in the PLA one. To the best of our knowledge, we present the first report referring the presence of confined water in a hydrophobic scaffold as PLA for tissue engineering. Our findings can provide new opportunities to understand the role of confined water in tissue engineering applications. For instance, we argue that PLA degradation may be affected the most by confined water. PLA degradation involves hydrolytic and enzymatic degradation reactions, which can both be sensitive to changes in water properties.
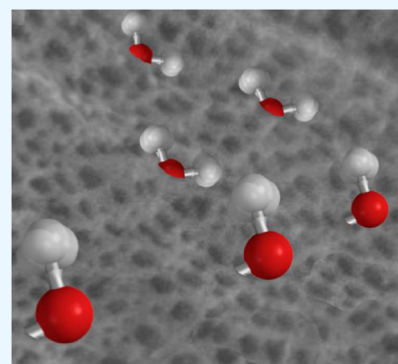
## ■ INTRODUCTION

Resorbable polylactic acid (PLA) ultrathin fibers have been employed as scaffolds for tissue engineering applications[1] due to its micro- and nanoporous structure that favors cell adhesion, besides inducing cell proliferation and upregulating gene expression related to tissue regeneration.[2]

The main advantages of PLA include its preparation using renewable sources (e.g., lactic acid obtained from microbial fermentation, followed by polymerization to produce PLA), its physical−chemical properties suitable for biomedical applications (e.g., hydrolytic degradation kinetics), and its nontoxic nor poluent degradation products. Besides, PLA has been approved by the FDA (Food and Drug Administration, USA) since the 1970s.[3]

Altogether, these characteristics of PLA make it favorable for applications in biomedicine. PLA outperforms synthetic polymers in stimulating cell functions such as cell attachment, growth, and differentiation due to its biocompatible characteristics.[3] However, PLA fibers are soft and weaker than those of synthetic polymers limiting their application as a scaffold for

tissue regeneration due to lower mechanical performance.[4] Adding fillers to the structure of PLA electrospun fibers has been an interesting approach to overcoming this limitation.

For example, multiwalled carbon nanotubes (CNTs) have been incorporated into electrospun fibers to improve its mechanical properties of the scaffold, such as elastic modulus and tensile strength, making them even more suitable for tissue engineering applications.[5]

The thermal behavior of PLA is also affected by the presence of CNTs as well as its crystallinity. Even in small amounts, the presence of CNTs makes PLA more hydrophobic, resulting in nanostructured, porous, and biocompatible polymeric scaffolds with a high surface area and with notable potential for tissue

engineering applications.[6] Similar to cellulose fibers, PLA fibers can be processed by electrospinning to obtain fibers with a tailored nanoporosity. For example, if PLA is dissolved in acetone before electrospinning, the obtained fiber shows a smooth surface; on the other hand, if PLA is dissolved in chloroform or a solution of chloroform and a nonpolar solvent, then surface nanoporosity is achieved after electrospinning.[7]

Interestingly, there are physical−chemical properties of the scaffold that enhance its biological performance such as nutrient transport, swelling, mechanical properties, mass transport for waste removal, hydration to allow biochemical reactions, and cell−matrix interaction[8] to name but a few.

From a physical−chemical perspective, the properties of scaffolds can be grouped into those influenced by mass transport or chemical reactions. For example, nutrient transport and waste removal are related to mass transport, while swelling, mechanical properties, cell−matrix interaction, and hydration are related to scaffold reactivity.[9] Regarding mass transport, it is needed to guarantee both oxygen and nutrient supply to the inner space of the scaffold so that cells can migrate and proliferate, allowing tissue regeneration. Besides, mass transport is needed to remove waste produced in metabolic functioning of the cells.[10]

Scaffolds should mechanically support cell growth and be degraded simultaneously with tissue growth. Hydration and swelling are factors related to scaffold degradation. Hydration is the ability of the scaffold to interact with and absorb water,[11] while swelling it refers to the scaffold's ability to swell upon water absorption within the scaffold microstructure. Hydration also interferes in the mechanical properties, as PLA shows hydrolytic degradation.[12] Therefore, water absorption critically affects catalysis and hydrolysis reactions.[9]

Either mass transport or chemical reactions are related to water properties, such as viscosity and reactivity. Interestingly, both properties can be influenced by confined water, which is defined as water that is confined or trapped within a confined space, such as small pores, nanoscale channels, or within the matrix of materials.[13,14] In fact, as pointed out by Wang et al.,[15] the unusual behaviors of the confined water depend strongly on the confinement size and the interaction between the molecules and confining surface. These diverse properties of confined water open a new door to materials science and may play an important role in the future development of biology. For more details concerning the intriguing properties of confined water and its impact on materials properties, consider refs 16−19.

Despite the influence of confined water in biomaterials science, there is a lack of studies evaluating its behavior in biomedical materials. Therefore, a large amount of the studies devoted to elucidating the behavior of confined water employed nanostructures that created confined spaces, such as nanoporous silica matrices,[20] vermiculite,[21] molecular sieves,[22] carbon nanotubes,[23] and mesoporous carbon[24] among others. However, these studies endow a better understanding of the structural and dynamic relaxation processes of confined water, not only at room temperature but also in its supercooled phase, where water-phase transitions are achievable, clarifying physical−chemical mechanisms of biomolecules and their biological activity.[25]

Confined water shows diverse behaviors on hydrophobic and hydrophilic surfaces. In hydrophilic cavities, the water condenses from the gaseous to the vitreous phase, generating at least four layers of absorbed water.[26] There is strong competition between polar interactions, surface hydrogen bonds, and hydrogen water−water bonds, which affects the reactivity of reactions happening nearby. In polymeric fibers, for example, surface-confined water in cellulose fibers catalyzes surface acetylation, increasing the reaction rate and efficiency by 8 times and 30%, respectively, compared with fibers free of confined water. Moreover, confined water enables control over the chemical accessibility of selected hydroxyl groups through the extent of hydration, allowing region-selective reactions, a major challenge in cellulose modification.[19]

When confined in cavities composed of hydrophobic surfaces, such as carbon nanotubes, the $\pi$ orbitals at the inner tube surface can be polarized by water molecules,[27] enabling faster proton transfer similar to proton channels in cells.[28] The enhancement of proton transfer within the scaffolds can favor pH-buffering needed for cell survival maintenance.[29] Besides, in hydrophobic cavities, the physical properties of water, including viscosity, can show an Arrhenius behavior related to high-to-low density liquid-phase transition, hydrogen bonding, and water diffusion.[22,30] However, Arrhenius's behavior is only noticed at low temperatures. For example, in carbon nanotubes, the crossover from non-Arrhenius to Arrhenius behavior occurred in $T \sim 190$ K. Nonetheless, when water properties are measured as a function of observing this crossover is an indicative of the presence of confined water in the system, which implies that detecting confined water in a system is much easier at low temperatures.[31,32]

Considering hydrolytic reactions in PLA, one may infer that the presence of confined water could catalyze them, increasing the scaffold degradation rate. In fact, the water confinement in hydrophobic PLA micro- and nanoporous fibers containing few amounts of CNT was not explored yet, to the best of our knowledge. In this way, herein, we have analyzed the confined water onto highly porous PLA microfibers containing a few amounts of incorporated CNT for the first time. We believe that understanding the water behavior in these scaffolds can favor the development of new scaffolds with tailored properties to enhance tissue regeneration in future applications.

## ■ METHODOLOGY

**PLA Nanofibers.** The PLA-containing CNT (PLA + CNT-O$_2$) is a composite material that contains small amounts of exfoliated CNTs after oxygen plasma treatment in rotationally spun fibers. PLA + CNT-O$_2$ fibers were prepared using the rotary-jet spinning method as described in detail elsewhere.[6,33] Briefly, 1 g of PLA (NatureWorks LLC, named Ingeo biopolymer 2003 D, with 4.3% of D-lactic acid monomer) pellets was dissolved in 8 mL of chloroform (Sigma-Aldrich). Separately, 0.1 g of CNT-O$_2$ (produced and functionalized as described in detail here[34]) was added into 2 mL of DCM and sonicated (Elmasonic S10H) for 1800 s. Finally, both solutions were thoroughly mixed using magnetic agitation (Ika, HS7) for 1800 s. Solutions were then rotary jet-spun using a homemade apparatus (described in detail here[6]). Briefly, its apparatus consisted of a perforated reservoir with an internal volume of 6 mL with two opposing orifices 0.3 mm in diameter, a static collector, a rotary tool (FERRARI MR30K) with varying frequency from 418 to 3141 rad/s, and a collector system onto which the fibers were deposited. The fibers were then rotary jet spun for 1800 s and kept under vacuum.

More details concerning the preparation of these samples including the experimental conditions for the production of

these fibers can be found in ref 6. Details concerning wettability, porosity, and surface area of this set of samples were also discussed in the last reference. Degradation studies, cytotoxicity, surface area, and porosity data for PLA samples without CNTs were published elsewhere.[35]

**Water Confinement.** The water confinement was performed under application of external hydrostatic pressures using a "homemade" Cu−Be pressure cell. Figure 1 shows the
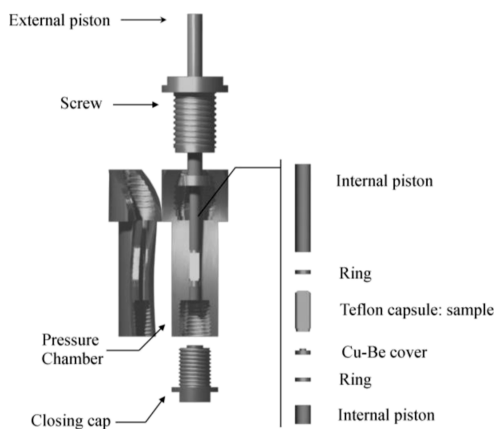


**Figure 1.** Scheme of a "homemade" Cu−Be pressure cell employed to confine water inside PLA + CNT-O$_2$ nanopores. The sample is placed in the Teflon capsule which is filled with water.

scheme of the cell. The Teflon capsule was filled with deionized water, and then the sample was inserted. Air bubbles were avoided. It was applied to 5 different values of external pressures in the interval of 1.50−5.52 MPa. After applying pressure, the cell was maintained under the respective pressure up to 15 min.

**Scanning Electron Microscopy.** Morphological characterization was performed using scanning electron microscopy (SEM) microscopy using the equipment Zeiss EVO MA 10 operating at 20.0 kV in a working distance of 11.0 mm. A thin gold layer of 10 nm was deposited by sputtering over samples prior to imaging of the surface topography.

Morphological pieces of information concerning the PLA samples using the methodology described here but without CNT and degradation studies as well could be found in ref 2.

**Fourier Transform Infrared Spectroscopy.** Infrared spectroscopy measurements were performed in a Varian 610 Fourier transform infrared (FTIR) spectroscopy microspectrometer coupled to a 640-IR FTIR spectrometer (LN$_2$ Ge detector) in reflectance mode. Spectra were obtained with the accumulation of 300 scans, in the range between 700 and 6000 cm$^{-1}$. Measurements were performed in a microscope coupled to FTIR in a 250 × 250 $\mu$m$^2$ region. The usage of a microscope warrants reproducibility of each measurement and fast focusing

in the case of thermal drift due to temperature changes. The amount of fibers in the spectral capturing window is ∼50. All measurements were made in triplicate, and the error bars are smaller than or equal to symbol size otherwise specified. Measurements were carried out in samples prepared under pressure (0−552 MPa) to increase the presence of confined water and the intensity of their vibrational modes.

Measurements as a function of temperature were performed adapting the spectrometer to an ultralow vibration He closed-circuit cryostat (CS-204SF-DMX-20-OM, Advanced Research Systems) which operates in the temperature range between 7 and 350 K. The first adaptation made was the replacement of the quartz window by a calcium fluoride one whose transmittance is close to 90% for infrared wavelengths. The cryostat was mounted on an optical jack that, in turn, was attached to an optical table equipped with a damping system. The use of the jack allowed a fine adjustment of the sample height since it is very important that the sample is in the focus of the excitation source. The spectra were obtained between 10 and 300 K (temperature variation $\Delta T$ = 10 K), with the accumulation of 300 scans, in the range between 700 and 6000 cm$^{-1}$. In order for the sample to have a good thermal coupling with the copper cold finger of the cryostat, silver glue was used. Spectral bands were deconvoluted to a sum of pseudo-Voigt line shapes using *fityk* software.[36]

## ■ RESULTS AND DISCUSSION

The SEM image of the PLA + CNT-O$_2$ scaffold (Figure 2) evidenced the uniform set of almost parallel fiber bundles. The mean diameter of the fibers was 7.5 $\mu$m (Figure 2b). Also, fibers showed surface nanoporosity of a mean pore size of 120 nm, as evidenced in the SEM image in Figure 2c. Thereby, microfiber scaffolds were obtained, and nanoporosity was achieved, which is proper for water confinement studies. Surface nanoporosity was achieved because we employed chloroform as the solvent of PLA. Huang et al.[7] already showed the mechanism of nanoporosity formation in PLA fibers. As electrospinning is performed at room temperature and in an open space, the water droplets from the air interact with the surface of the PLA fibers upon chloroform evaporation, forming these cavities.

The PLA surface is hydrophobic, having a static water contact angle in the range of 75−85°. Thus, water is confined here present on borders of hydrophobic cavities, and the corresponding behavior would be similar to those observed on liquid−gas interfaces except that the confinement prevents the free movement of water to the surface, and van der Waals interactions direct the external molecules to preferred directions with respect to the atoms in surface. As pointed out by Li et al.,[18] the experimental investigations of water on hydrophobic surfaces at a microscopic level are still lacking because of the weak surface adsorption of water on a
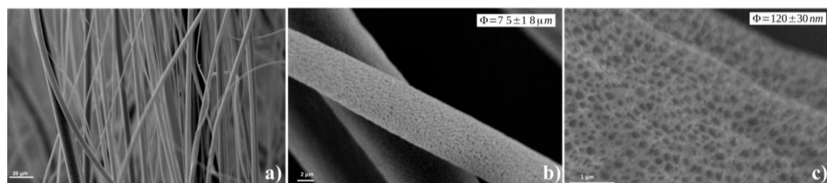


**Figure 2.** Representative SEM micrographs of PLA + CNT-O$_2$ fibers showing typical fiber bundles (a), diameters (average diameter $\Phi$ = 7.5 ± 1.8 $\mu$m, b), and porous (average size $\Phi$ = 120 ± 30 nm, c).

hydrophobic substrate. Liquid-like water nanodroplets with sizes between 10 and 100 nm have been reported on hydrophobic surfaces as graphene and mica at step edges and surface defects (see, e.g., refs 37 and 38).

FTIR was used to characterize the structure of PLA + CNT-$O_2$ fibers and to check the presence of water upon applying different pressures. We notice that a complete set of PLA-assigned bands of PLA (Table 1) was observed in our samples.

**Table 1. Assignments of the IR Bands of the Semi-crystalline PLLA[42]**

| wavenumber (cm$^{-1}$) | intensity | band assignment |
|---|---|---|
| 3571 | weak | stretching OH (free) |
| 2997 | average | asymmetrical stretching $CH_3$ |
| 2947 | average | symmetrical stretching $CH_3$ |
| 2882 | weak | stretching CH |
| 1817−1716 | very strong | stretching C=O |
| 1452 | strong | bending asymmetric $CH_3$ |
| 1348, 1388 | strong | bending symmetric $CH_3$ |
| 1368 | strong | bending CH + bending symmetric $CH_3$ |
| 1360 | strong | bending CH + bending symmetric $CH_3$ |
| 1300, 1313 | average | bending CH |
| 1270 | strong | bending CH + stretching COC |
| 1215 | very strong | asymmetrical stretching COC |
| 1185 | very strong | asymmetrical stretching COC |
| 1130 | strong | rocking asymmetric $CH_3$ |
| 1090 | very strong | symmetrical stretching COC |
| 1045 | strong | stretching C−$CH_3$ |
| 960 | weak | rocking $CH_3$ + stretching CC |
| 925 | weak | rocking $CH_3$ + stretching CC |
| 875 | average | stretching C−COO |
| 760 | weak | bending C = 0 |
| 740 | shoulder | bending C = 0 |
| 715 | average | stretching C=O |
| 695 | average | stretching C=O |

This spectroscopic technique has been applied to detect and investigate the local environmental of confined water in diverse materials. For example, Richard et al.[39] probed confined water on micrometric-sized mineral grain powders and mesoporous silica MCM-41. They were able to distinguish different water types, including free and capillary water, from confined and adsorbed water. On the other hand, Baumgartner et al.[40] probed the structure of water adsorbed from the gas phase into silica mesopores at different water vapor pressures using mid-infrared attenuated total reflection spectroscopy. They showed that quantitative analysis of the water bending vibration at 1640 cm$^{-1}$ at varying vapor pressures allows for retrieving porosity and pore size distribution of the mesoporous films. Hydrogen bonding of water in high-density, unordered bulk, low-density, and surface-induced ordered water was also successfully detected and investigated as a function of monolayers. The interactions of water in a heterogeneous confining environment within a prototype of pillared layer-type metal−organic frameworks (MOFs), CPL-1 ([$Cu_2(pzdc)_2(pyz)$]$_n$, where pzdc = 2,3-pyrazinedicarboxylate and pyz = pyrazine) were studied by Hiraoka et al. using Raman, FTIR, and IR electroabsorption techniques.[41] The FTIR data and corresponding analysis performed by these authors indicated accurate assignments of the framework of carboxylate vibrational modes associated with water-filled and empty nanopores of the MOF.

The spectra obtained for samples submitted to different pressures are shown in Figure 3. The qualitative analysis of the integrated area of the confined water bands ∼1930−2030 and 5200 cm$^{-1}$ (indicated by the arrows in Figure 3) demonstrated that the pressure $P = 4.50$ MPa induced the incorporation of an increasing amount of water molecules in the pores. The higher applied pressure ($P = 5.52$ MPa) probably caused structural damage to the PLA + CNT-$O_2$ fibers since the spectrum showed major changes in relation to the others. Comparing 4.50 and 5.52 MPa spectra, the disappearance of 1232, 1790, 2480−2760, and 3220 cm$^{-1}$ bands at 5.52 MPa pressure is clear. The remaining bands presented different relative intensity ratios comparing both spectra. These changes are unambiguous signatures of structural changes in PLA.

Figure 4 shows that the spectrum of PLA + CNT-$O_2$ fibers at 0 MPa is compared with that under 4.50 MPa. In the
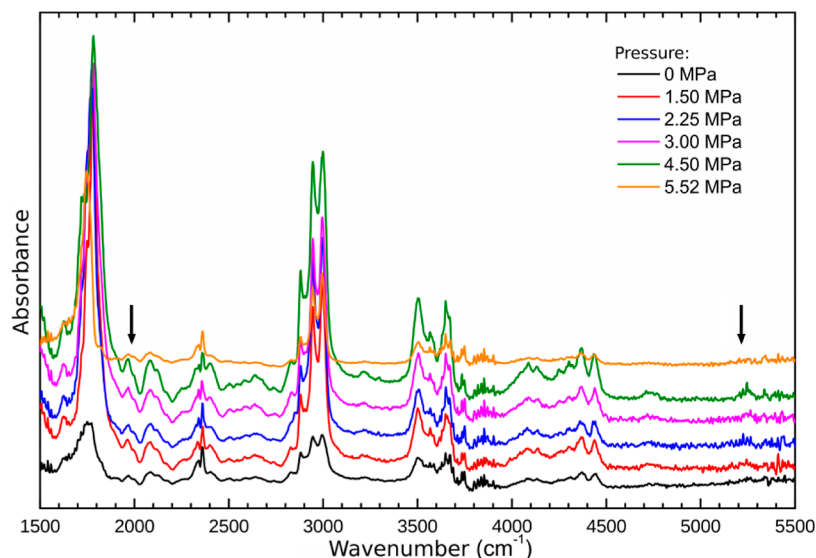


**Figure 3.** FTIR spectrum, in the interval between 1500 and 5500 cm$^{-1}$, of PLA + CNT-$O_2$ samples subjected to different pressures at room temperature. Arrows indicate the bands related to the vibrations of the water molecule.
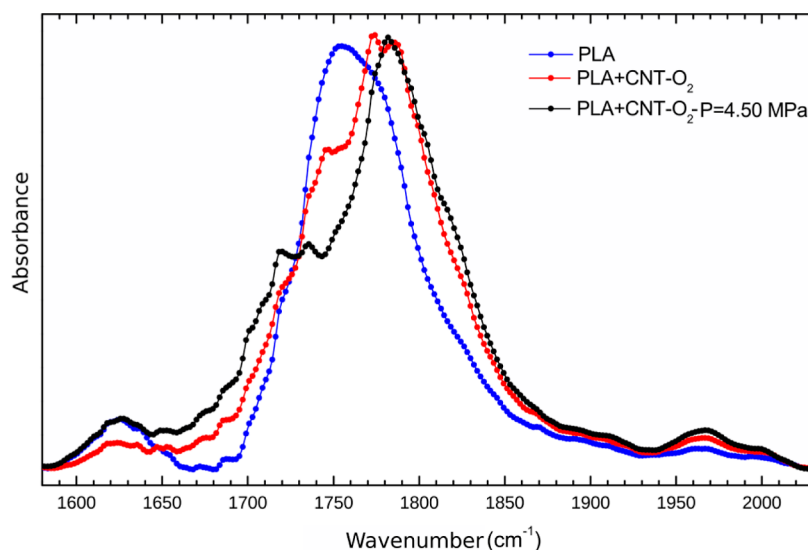
**Figure 4.** FTIR spectrum at room temperature in the interval between ~1600 and 2050 cm$^{-1}$, of the samples of pure PLA, PLA + CNT-O$_2$, and PLA + CNT-O$_2$ subjected to the pressure that induced the greatest incorporation of water molecules.

interval between ~1500 and 2800 cm$^{-1}$, semicrystalline PLA presents only band at 1760 cm$^{-1}$ (see Table 1), which corresponds to the stretching of C=O. However, the presence of water generates hydrogen bonds' water molecules and C=O group of the PLA, which would result in new modes of vibration (see Figure 4). These new modes can also be noticed in Figure 5, where peak energies were tracked as a function of
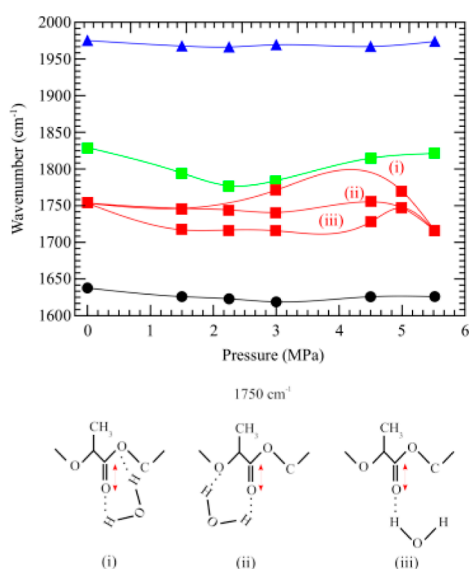


**Figure 5.** Pressure dependence of some band energies between 1600 and 2000 cm$^{-1}$. Solid lines are guide-to-the eyes splines. Below, proposed configurations for the carbonyl and water molecule environment.

applied pressure. Above 1 MPa, extra bands are noticed around the band at 1750 cm$^{-1}$ (red lines). We elaborate that these extra bands are associated with 3 different configurations of water interaction with polyester bonds.

However, to clarify this point, independent verification is needed, e.g., perform molecular dynamics simulations and vibrational calculations on the PLA structure exposed to confined water and make previsions concerning these bands.

According to the analysis presented above, infrared spectroscopy measurements were made only for the sample submitted to pressure P = 3.75 MPa at different temperatures, varying between 10 and 300 K, to investigate the liquid−liquid transition of the confined water present in the pores of the PLA microfibers. This pressure was chosen to guarantee that water was incorporated in the surface nanopores of PLA without causing structural changes to the scaffold.

Figure 6 presents all spectra obtained as a function of the temperature. The phonon line shape has enough pieces of information to resolve dynamics of a specific vibration. In particular, the thermal behavior of line width of specific vibrations is able to decaying channels where that specific functional group is actuating (see, e.g., ref 43). We notice that the spectral intensity in the region of 5200 cm$^{-1}$ became low and noisy, then only the water bands in the interval ~1600−2060 cm$^{-1}$ were analyzed. Figure 7 shows 4 spectra at selected temperatures (10, 100, 200, and 300 K) to illustrate the evolution in profile change of the C=O stretching bands of the PLA in the region ~1600−2000 cm$^{-1}$. After deconvolution of the C=O stretching bands, only the behavior of the bands at 1743, 1767, 1783, 1820, 1967, and 2055 cm$^{-1}$ was analyzed in more detail. The dependence of the frequency of these bands on the temperature is shown in Figure 8. It is noticed that 1716, 1743, 1783, and 1820 cm$^{-1}$ are observable regardless of the temperature, while bands at 1767 and 1739 cm$^{-1}$ are only observable at T < 100 K. It suggests that some configurations of interaction between water molecules and C=O bonds are restricted to low-temperature ranges, and a subtle structural transition is established at T ~ 100 K.

The mechanism by which phonons in a solid can be scattered explaining its temperature dependence is the anharmonic Umklapp process including boundary, phonon impurity, electron−phonon, or phonon−phonon scatterings.[44] Each of these mechanisms is associated with the relaxation time, which is inversely proportional to their relaxation rate. The total relaxation rate of a phonon is given by Matthiessen's rule $\tau^{-1} = \sum \tau^{-1}$. Usually, the temperature dependence of optical phonons is dominated by phonon−phonon anharmonic decay. In spectroscopy, it can be studied by evaluating the full width at half-maximum ($\Gamma$) of a peak as $\tau \propto \Gamma$.[45] By
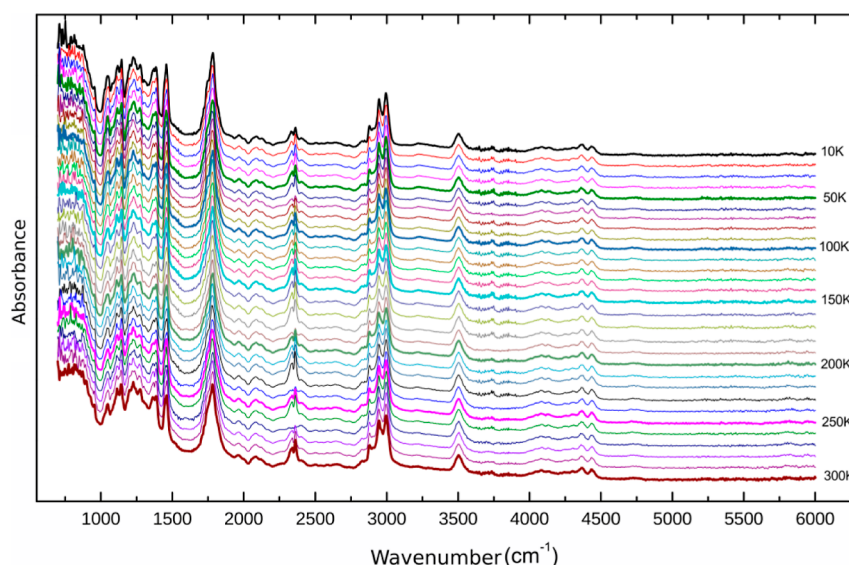
**Figure 6.** FTIR spectra of the PLA + CNT-O$_2$ microfibers as a function of temperature.
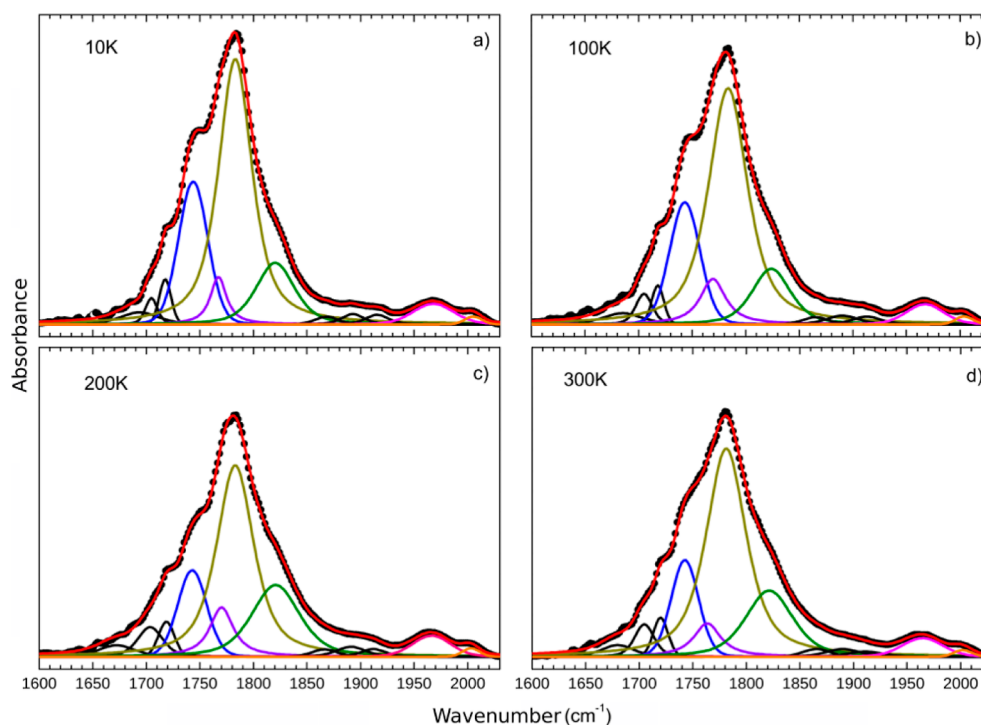


**Figure 7.** Experimental data (●) in the region 1600−2050 cm$^{-1}$ fitted to a sum of pseudo-Voigt line shapes for 4 selected temperatures (a) 10, (b) 100, (c) 200, and (d) 300 K. The solid lines represent the deconvoluted bands. The total contribution of the bands is also represented.

evaluating $\Gamma$, it is possible to study whether a specific band is related to physical phenomena that cause changes in $\Gamma$, which is the case of confined water.

The relaxation behavior of confined water is generally described by the viscosity-related main relaxation process ($\alpha$-kind) and one or several secondary relaxation processes ($\beta$-kind). For $\alpha$ processes, $\tau_\alpha$ usually displays some degree of non-Arrhenius (or fragile) temperature dependence[46] being well described by the Vogel−Fulcher−Tammann law. The phonon relaxation rate, in this case, will be[46]

$$\Gamma_{non-Arr} = \Gamma_{two-ph}(1 + e^{-BT_0/T-T_0}) \qquad (1)$$

where $\Gamma_{two-ph}$ is a constant related to the residual two-phonon anharmonic decay, $B$ is a constant that measures fragility, and $T_0$ is the ideal glass-transition temperature. The Arrhenius (or strong) temperature dependence will be

$$\Gamma_{Arr} = \Gamma_{two-ph}(1 + e^{-E_A/k_B T}) \qquad (2)$$

where $E_A$ is the activation energy for the relaxation process and $k_B$ is the Boltzmann constant.

Figure 9 shows the temperature dependence of $\Gamma$ for bands at 1716, 1735, 1764, 1786, and 1817 cm$^{-1}$. While bands at 1735, 1786, and 1764 cm$^{-1}$ presented no evidence of non-Arrhenius to Arrhenius crossover, those bands at 1716 and 1817 cm$^{-1}$ showed a crossover at $T \sim 190$ K. This transition is
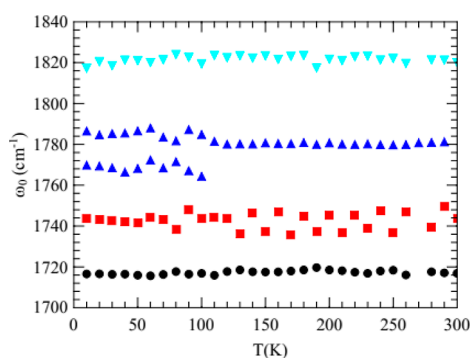
**Figure 8.** Temperature dependence of frequency of the interaction modes between C=O and water.
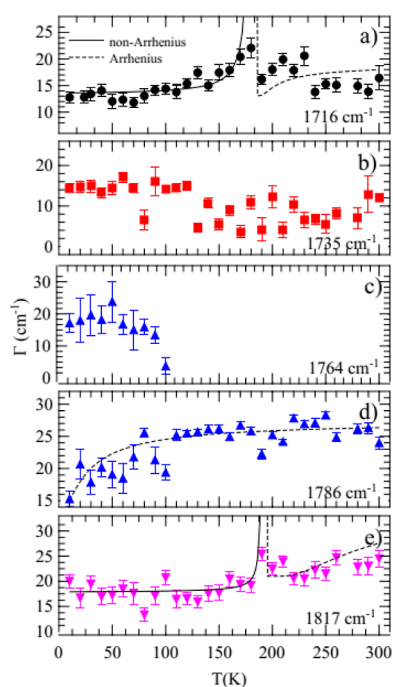


**Figure 9.** Temperature dependence of fwhm ($\Gamma$) of the interaction modes between C=O and water (a) 1743, (b) 1667, (c) 1783, and (d,e) 1820 cm$^{-1}$. Solid and dashed black lines are the fitting to non-Arrhenius (eq 1) and Arrhenius (eq 2) dependence.

evidenced by non-Arrhenius ($T < 190$ K) and Arrhenius ($T > 190$ K) fitting to the experimental data of 1716 and 1817 cm$^{-1}$ bands. The corresponding ideal glass-transition temperature was found to be $T_0 = 190 \pm 5$ K in both cases. The activation energy was $E_A = 230 \pm 20$ kcal/mol. The change from non-Arrhenius to Arrhenius behavior is typical of confined water, meaning that confined water is found at the PLA + CNT-O$_2$ pores.

As mentioned in the introduction section, several properties of a scaffold can be influenced by the presence of confined water, including hydration, nutrient transport, cell–matrix interaction, swelling, mechanical properties, waste removal, and degradation rate. Among these properties, the degradation rate may be the most influenced by confined water at the surface nanopores. The initial degradation of PLA fibers includes its hydration and surface protonation of carboxylic acid end groups, which causes the autocatalytic degradation of polyesters.[47] The maintenance of autocatalytic degradation of PLA depends on the diffusion of hydronium species and the

leached monomer, ultimately causing the mass loss of the scaffold.[48] Considering that confined water changes the viscosity and mass transport properties in the confined space,[49] it is expected that the existence of confined water may influence the degradation rate of PLA scaffolds. It is worth noting that the reactivity of acetylation reactions at nanoporous cellulose fibers changes with the presence of confined water;[19] thereby, it is reasonable to assume that the reactivity of other reactions may change in other polymeric fibers that display confined cavities.

Besides, PLA scaffolds also undergo enzymatic degradation.[49] It is known that confined water also changes the reactivity of enzymes in confined cavities. For example, under hydrated, confined cavities, lysozymes show different hydration levels and activation energy of enzymatic reaction.[50] Although PLA is mainly degraded by proteases like proteinase K and cutinase-type enzyme,[49] which are not lysozymes, it is still possible that their reactivity may change under confined cavities.

Overall, the properties of water under confined spaces have been underestimated in the field of biomaterials science. Most of the studies that have modeled the degradation rate of PLA-electrospun fibers, either by degradation experiments or by computational dynamic simulations,[47,48] have not considered a possible effect of confined water on the mechanisms of PLA degradation. Thus, the results presented in this work can help future works to model the degradation rate of PLA fibers with surface nanoporosities.

## ■ CONCLUSIONS

PLA + CNT-O$_2$ fiber scaffolds were obtained by electro-spinning, whose surface contained nanopores. The existence of confined water in these scaffolds was evaluated by FTIR spectroscopy. A hydrostatic pressure was applied to the fibers to enhance the intermolecular interactions between water molecules and C=O groups from polyester bonds, which were evaluated over the wavenumber between 1600 and 2000 cm$^{-1}$. The analysis of temperature dependence of FTIR spectra indicated the presence of confined water characterized by a non-Arrhenius to Arrhenius behavior in the deconvoluted bands at 1817 and 1716 cm$^{-1}$. To the best of our knowledge, we present the first report referring the presence of confined water in a scaffold for tissue engineering. Our findings can open new opportunities to understand the role of confined water in tissue engineering applications. For instance, we believe that PLA degradation may be affected the most by confined water. PLA degradation involves hydrolytic and enzymatic degradation reactions, which can be both sensitive to changes in water properties. Notwithstanding, the presence of confined water might be present in other scaffolds that show confined cavities at the nanoscale, and new studies to evaluate their presence should be encouraged, as it is new and unclear whether confined water displays a fundamental role in tissue engineering applications.

## ■ AUTHOR INFORMATION

### Corresponding Author

**Herculano Martinho** − *Federal University of ABC, Santo André, São Paulo 09280-560, Brazil;* ⊙ orcid.org/0000-0002-7690-014X; Email: herculano.martinho@ufabc.edu.br

## Authors

**Mariana Ishikawa** — *Federal University of ABC, Santo André, São Paulo 09280-560, Brazil*

**Roger Borges** — *Federal University of ABC, Santo André, São Paulo 09280-560, Brazil; School of Biomedical Engineering, Faculdade Israelita de Cîencias da Saúde Albert Einstein, Hospital Israelita Albert Einstein, São Paulo, São Paulo 09280-560, Brazil*

**André Mourão** — *Federal University of ABC, Santo André, São Paulo 09280-560, Brazil*

**Letície Mendonça Ferreira** — *Federal University of ABC, Santo André, São Paulo 09280-560, Brazil*

**Anderson O. Lobo** — *Interdisciplinary Laboratory for Advanced Materials, BioMatLab, Department of Materials Engineering, Federal University of Piauí, Teresina, Piauí 64049-550, Brazil;* ⓞ orcid.org/0000-0002-2544-0438

Complete contact information is available at:
https://pubs.acs.org/10.1021/acsomega.3c08057

## Notes

The authors declare no competing financial interest.

## ■ REFERENCES

(1) Gupta, B.; Revagade, N.; Hilborn, J. Poly (lactic acid) fiber: an overview. *Prog. Polym. Sci.* **2007**, *32*, 455−482.

(2) Zamproni, L. N.; Grinet, M. A.; Mundim, M. T.; Reis, M. B.; Galindo, L. T.; Marciano, F. R.; Lobo, A. O.; Porcionatto, M. Rotary jet-spun porous microfibers as scaffolds for stem cells delivery to central nervous system injury. *Nanomed.: Nanotechnol. Biol. Med.* **2019**, *15*, 98−107.

(3) Zarrintaj, P.; Zangene, E.; Manouchehri, S.; Amirabad, L. M.; Baheiraei, N.; Hadjighasem, M. R.; Farokhi, M.; Ganjali, M. R.; Walker, B. W.; Saeb, M. R.; Mozafari, M.; Thomas, S.; Annabi, N. Conductive biomaterials as nerve conduits: recent advances and future challenges. *Appl. Mater. Today* **2020**, *20*, 100784.

(4) Ghosal, K.; Agatemor, C.; Špitálsky, Z.; Thomas, S.; Kny, E. Electrospinning tissue engineering and wound dressing scaffolds from polymer-titanium dioxide nanocomposites. *Chem. Eng. J.* **2019**, *358*, 1262−1278.

(5) Liu, F.; Guo, R.; Shen, M.; Wang, S.; Shi, X. Effect of processing variables on the morphology of electrospun poly[(lactic acid)-co-(glycolic acid)] nanofibers. *Macromol. Mater. Eng.* **2009**, *294*, 666−672.

(6) Andrade, P. O.; Grinet, M. A. V. M.; Costa, M. M.; Santo, A. M. E.; Marciano, F. R.; Lobo, A. O. Poly (lactic acid) fine fibers containing a low content of superhydrophilic multi-walled carbon nanotube graphene oxide hybrid as scaffolds for biological applications. *Macromol. Mater. Eng.* **2018**, *303*, 1800317.

(7) Huang, C.; Thomas, N. Fabricating porous poly(lactic acid) fibres via electrospinning. *Eur. Polym. J.* **2018**, *99*, 464−476.

(8) Loh, Q. L.; Choong, C. Three-dimensional scaffolds for tissue engineering applications: role of porosity and pore size. *Tissue Eng., Part B* **2013**, *19*, 485−502.

(9) Vikingsson, L.; Claessens, B.; Gómez-Tejedor, J.; Gallego Ferrer, G.; Gómez Ribelles, J. Relationship between micro-porosity, water permeability and mechanical behavior in scaffolds for cartilage engineering. *J. Mech. Behav. Biomed. Mater.* **2015**, *48*, 60−69.

(10) Op Den Buijs, J.; Dragomir-Daescu, D.; Ritman, E. L. Cyclic deformation-induced solute transport in tissue scaffolds with computer designed, interconnected, pore networks: experiments and simulations. *Ann. Biomed. Eng.* **2009**, *37*, 1601−1612.

(11) Hidalgo, I. A.; Sojo, F.; Arvelo, F.; Sabino, M. A. Functional electrospun poly (lactic acid) scaffolds for biomedical applications: experimental conditions, degradation and biocompatibility study. *Mol. Cell. Biomech.* **2013**, *10*, 85−105.

(12) Dias, J. C.; Ribeiro, C.; Sencadas, V.; Botelho, G.; Ribelles, J. G.; Lanceros-Mendez, S. Influence of fiber diameter and crystallinity on the stability of electrospun poly (l-lactic acid) membranes to hydrolytic degradation. *Polym. Test.* **2012**, *31*, 770−776.

(13) Swenson, J.; Jansson, H.; Bergman, R. Relaxation processes in supercooled confined water and implications for protein dynamics. *Phys. Rev. Lett.* **2006**, *96*, 247802.

(14) Swenson, J. The glass transition and fragility of supercooled confined water. *J. Phys.: Condens. Matter* **2004**, *16*, S5317−S5327.

(15) Wang, D.; Tian, Y.; Jiang, L. Abnormal properties of low-dimensional confined water. *Small* **2021**, *17*, 2100788.

(16) Munoz-Santiburcio, D.; Marx, D. Confinement-controlled aqueous chemistry within nanometric slit pores: focus review. *Chem. Rev.* **2021**, *121*, 6293−6320.

(17) Jackson, G. L.; Kim, S. A.; Jayaraman, A.; Diallo, S. O.; Mahanthappa, M. K. Consequences of convex nanopore chemistry on confined water dynamics. *J. Phys. Chem. B* **2020**, *124*, 1495−1508.

(18) Li, Q.; Song, J.; Besenbacher, F.; Dong, M. Two-dimensional material confined water. *Acc. Chem. Res.* **2015**, *48*, 119−127.

(19) Beaumont, M.; Jusner, P.; Gierlinger, N.; King, A. W.; Potthast, A.; Rojas, O. J.; Rosenau, T. Unique reactivity of nanoporous cellulosic materials mediated by surface-confined water. *Nat. Commun.* **2021**, *12*, 2513.

(20) (a) Liu, L.; Chen, S.-H.; Faraone, A.; Yen, C.-W.; Mou, C.-Y. Pressure dependence of fragile-to-strong transition and a possible second critical point in supercooled confined water. *Phys. Rev. Lett.* **2005**, *95*, 117802. (b) Faraone, A.; Liu, L.; Mou, C.-Y.; Yen, C.-W.; Chen, S.-H. Fragile-to-strong liquid transition in deeply supercooled confined water. *J. Chem. Phys.* **2004**, *121*, 10843−10846.

(21) Bergman, R.; Swenson, J. Dynamics of supercooled water in confined geometry. *Nature* **2000**, *403*, 283−286.

(22) Swenson, J.; Jansson, H.; Howells, W.; Longeville, S. Dynamics of water in a molecular sieve by quasielastic neutron scattering. *J. Chem. Phys.* **2005**, *122*, 84505.

(23) Chakraborty, S.; Kumar, H.; Dasgupta, C.; Maiti, P. K. Confined water: structure, dynamics, and thermodynamics. *Acc. Chem. Res.* **2017**, *50*, 2139−2146.

(24) Ito, K.; Faraone, A.; Tyagi, M.; Yamaguchi, T.; Chen, S.-H. Nanoscale dynamics of water confined in ordered mesoporous carbon. *Phys. Chem. Chem. Phys.* **2019**, *21*, 8517−8528.

(25) Doster, W.; Cusack, S.; Petry, W. Dynamical transition of myoglobin revealed by inelastic neutron scattering. *Nature* **1989**, *337*, 754−756.

(26) Richard, T.; Mercury, L.; Poulet, F.; d'Hendecourt, L. Diffuse reflectance infrared Fourier transform spectroscopy as a tool to characterise water in adsorption/confinement situations. *J. Colloid Interface Sci.* **2006**, *304*, 125−136.

(27) Vaitheeswaran, S.; Rasaiah, J.; Hummer, G. Electric field and temperature effects on water in the narrow nonpolar pores of carbon nanotubes. *J. Chem. Phys.* **2004**, *121*, 7955−7965.

(28) Gileadi, E.; Kirowa-Eisner, E. Electrolytic conductivity the hopping mechanism of the proton and beyond. *Electrochim. Acta* **2006**, *51*, 6003−6011.

(29) Monfoulet, L.-E.; Becquart, P.; Marchat, D.; Vandamme, K.; Bourguignon, M.; Pacard, E.; Viateau, V.; Petite, H.; Logeart-Avramoglou, D. The pH in the microenvironment of human mesenchymal stem cells is a critical factor for optimal osteogenesis in tissue-engineered constructs. *Tissue Eng., Part A* **2014**, *20*, 1827−1840.

(30) Mallamace, F.; Branca, C.; Broccio, M.; Corsaro, C.; Gonzalez-Segredo, N.; Spooren, J.; Stanley, H.; Chen, S.-H. Transport

properties of supercooled confined water. *Eur. Phys. J.: Spec. Top.* **2008**, *161*, 19−33.

(31) Faraone, A.; Liu, K.-H.; Mou, C.-Y.; Zhang, Y.; Chen, S.-H. Single particle dynamics of water confined in a hydrophobically modified MCM-41-S nanoporous matrix. *J. Chem. Phys.* **2009**, *130*, 134512.

(32) Chu, X.-Q.; Kolesnikov, A.; Moravsky, A.; Garcia-Sakai, V.; Chen, S.-H. Observation of a dynamic crossover in water confined in double-wall carbon nanotubes. *Phys. Rev. E* **2007**, *76*, 021505.

(33) Lobo, A. O.; Zanin, H.; Siqueira, I. A.; Leite, N. C.; Marciano, F. R.; Corat, E. J. Effect of ultrasound irradiation on the production of nHAp/MWCNT nanocomposites. *Mater. Sci. Eng., C* **2013**, *33*, 4305−4312.

(34) Ricci, R.; Leite, N.; Da-Silva, N.; Pacheco-Soares, C.; Canevari, R.; Marciano, F.; Webster, T.; Lobo, A. Graphene oxide nanoribbons as nanomaterial for bone regeneration: effects on cytotoxicity, gene expression and bactericidal effect. *Mater. Sci. Eng. C* **2017**, *78*, 341−348.

(35) Zamproni, L. N.; Grinet, M. A.; Mundim, M. T.; Reis, M. B.; Galindo, L. T.; Marciano, F. R.; Lobo, A. O.; Porcionatto, M. Rotary jet-spun porous microfibers as scaffolds for stem cells delivery to central nervous system injury. *Nanomed. Nanotechnol. Biol. Med.* **2019**, *15*, 98−107.

(36) Wojdyr, M. Fityk: a general-purpose peak fitting program. *J. Appl. Crystallogr.* **2010**, *43*, 1126−1128.

(37) Rezania, B.; Dorn, M.; Severin, N.; Rabe, J. Influence of graphene exfoliation on the properties of water-containing adlayers visualized by graphenes and scanning force microscopy. *J. Colloid Interface Sci.* **2013**, *407*, 500−504.

(38) Cao, P.; Xu, K.; Varghese, J. O.; Heath, J. R. The microscopic structure of adsorbed water on hydrophobic surfaces under ambient conditions. *Nano Lett.* **2011**, *11*, 5581−5586.

(39) Richard, T.; Mercury, L.; Poulet, F.; d'Hendecourt, L. Diffuse reflectance infrared Fourier transform spectroscopy as a tool to characterise water in adsorption/confinement situations. *J. Colloid Interface Sci.* **2006**, *304*, 125−136.

(40) Baumgartner, B.; Hayden, J.; Loizillon, J.; Steinbacher, S.; Grosso, D.; Lendl, B. Pore size-dependent structure of confined water in mesoporous silica films from water adsorption/desorption using ATR−FTIR spectroscopy. *Langmuir* **2019**, *35*, 11986−11994.

(41) Hiraoka, T.; Shigeto, S. Interactions of water confined in a metal−organic framework as studied by a combined approach of Raman, FTIR, and IR electroabsorption spectroscopies and multivariate curve resolution analysis. *Phys. Chem. Chem. Phys.* **2020**, *22*, 17798−17806.

(42) Gonçalves, C.; Coutinho, J.; Marrucho, I. M.; et al. *Optical Properties*; Wiley Online Library, 2010.

(43) Perakis, F.; De Marco, L.; Shalit, A.; Tang, F.; Kann, Z. R.; Kuhne, T. D.; Torre, R.; Bonn, M.; Nagata, Y. Vibrational spectroscopy and dynamics of water. *Chem. Rev.* **2016**, *116*, 7590−7607.

(44) Dove, M. T. *Introduction to Lattice Dynamics*; Cambridge University Press, 1993; Vol. *4*, Chapter 8.

(45) Balkanski, M.; Wallis, R.; Haro, E. Anharmonic effects in light scattering due to optical phonons in silicon. *Phys. Rev. B* **1983**, *28*, 1928−1934.

(46) Grzybowska, K.; Paluch, M.; Grzybowski, A.; Pawlus, S.; Ancherbak, S.; Prevosto, D.; Capaccioli, S. Dynamic crossover of water relaxation in aqueous mixtures: effect of pressure. *J. Phys. Chem. Lett.* **2010**, *1*, 1170−1175.

(47) Mitchell, M. K.; Hirt, D. E. Degradation of PLA fibers at elevated temperature and humidity. *Polym. Eng. Sci.* **2015**, *55*, 1652−1660.

(48) Zhang, T.; Chen, H.; Guo, X.; Yu, Y.; Wulamu, A. A structure dynamic interaction multiscale method for degradation modeling of bioresorbable polyesters. *Polym. Degrad. Stab.* **2021**, *192*, 109704.

(49) Zaaba, N. F.; Jaafar, M. A review on degradation mechanisms of polylactic acid: hydrolytic, photodegradative, microbial, and enzymatic degradation. *Polym. Eng. Sci.* **2020**, *60*, 2061−2075.

(50) Mallamace, F.; Broccio, M.; Corsaro, C.; Faraone, A.; Wanderlingh, U.; Liu, L.; Mou, C.; Chen, S. The fragile-to-strong dynamic crossover transition in confined water: nuclear magnetic resonance results. *J. Chem. Phys.* **2006**, *124*, 161102.